Decarburization of 60Si2MnA in 20 Pct H_2O-N_2 at 700 °C to 900 °C

YISHENG R. CHEN, FAN ZHANG, and YU LIU

The decarburization behavior of a spring steel 60Si2MnA at 700 °C to 900 °C was examined. It was observed that after holding for 20 minutes in 20 pct H_2O-N_2, thick ferrite layers developed within 750 °C to 877 °C with a maximum thickness of about 100 μm observed at 805 °C to 825 °C, while the ferrite layers were much thinner at 900 °C and 700 °C. Carbon permeability analysis and theoretical calculation were conducted to assess the possibility of forming a ferrite layer. In the permeability analysis, several factors were considered: (1) carbon concentration at the steel surface, which was very likely determined by reaction equilibrium between FeO and dissolved carbon in steel, (2) carbon solubility in ferrite which had a maximum value at about 715 °C, and (3) carbon diffusivity in the ferrite phase. In the ferrite layer thickness calculation, the contribution from carbon diffusion in the austenite phase was also taken into account. While the carbon permeability analysis and ferrite layer thickness calculation showed good successes in predicting the pattern of ferrite layer thickness change with temperature, under the assumption of FeO-ferrite equilibrium the calculated ferrite layer thicknesses at 780 °C to 840 °C did not match the observed values well. Factors contributing to the discrepancy were discussed.

I. INTRODUCTION

THE steel grade 60Si2MnA with the specified composition ranges of C: 0.56 to 0.64 wt pct (weight percent), Si: 1.50 to 2.00 wt pct, Mn: 0.50 to 0.80 wt pct and Cr: ≤ 0.25 wt pct[1] is a commonly used high-strength spring steel in China. Its equivalent grades in some other countries are ASTM A29 - 9254 (Si: 1.2 to 1.6 pct), ASTM A29-9260 (Si: 1.80 to 2.20 pct),[2] BS EN 10089:2002 - 61SiCr7,[3] JIS G 4801-SUP6 (Si: 1.5 to 1.8 pct) and JIS G 4801-SUP7 (Si: 1.8 to 2.2). Due to its high-silicon content, this steel was susceptible to decarburization during steel processing at high temperatures, which greatly compromised its fatigue properties and service life.[4,5] There were many studies conducted recently to understand the decarburization mechanism of this steel to develop methods to combat the decarburization problem.[6–17] One important finding of these studies was that severe decarburization occurred at a temperature range below 900 °C, forming a thick ferrite layer on the steel surface. This observation was contradictory to the early claim by Birks et al.[18–21] that when a ferrite layer formed, the decarburization rate would be significantly reduced due to the low-carbon concentration in ferrite. In addition, a consensus could not be reached on the most sensitive decarburization temperature, with some proposing 750 °C[7–12,16,17] and others showing a temperature around 850 °C.[6,13–15]

The current study was, therefore, designed to examine the decarburization behavior of 60Si2MnA within the range of 700 °C to 900 °C to clarify the most sensitive decarburization temperature, and more importantly to understand the reason why the decarburization rate was not decreased when a ferrite layer formed, and identify the main factors that had determined the formation of a thick ferrite layer observed. An attempt was also made to develop a method to calculate the ferrite layer thickness using the new understandings arrived in the current study and existing diffusion theories and available data.

II. EXPERIMENTAL DETAILS

A ϕ16 mm wire sample provided by Zenith Special Steel Co. Ltd, China, was used for the experiments. The steel composition is shown in Table I. The sample was first pickled in an inhibited HCl solution to remove the oxide scale and then cut into 0.5 to 2 mm-thick disk-shaped specimens. The specimens were then ground to 1000 grit finish and cleaned using methanol prior to

YISHENG R. CHEN is with Steel Research Australia, 20 The Crescent, Springvale, VIC, 3171, Australia. Contact e-mail: yche6333@bigpond.net.au FAN ZHANG is with CompuTherm LLC, 8401 Greenway Blvd., Suite 248, Middleton, WI 53562. YU LIU is with Zenith Steel, No. 1, Zhongwu Avenue, Wujin District, Changzhou City, Jiangsu Province, China.
Manuscript submitted October 7, 2019.
Article published online January 31, 2020.

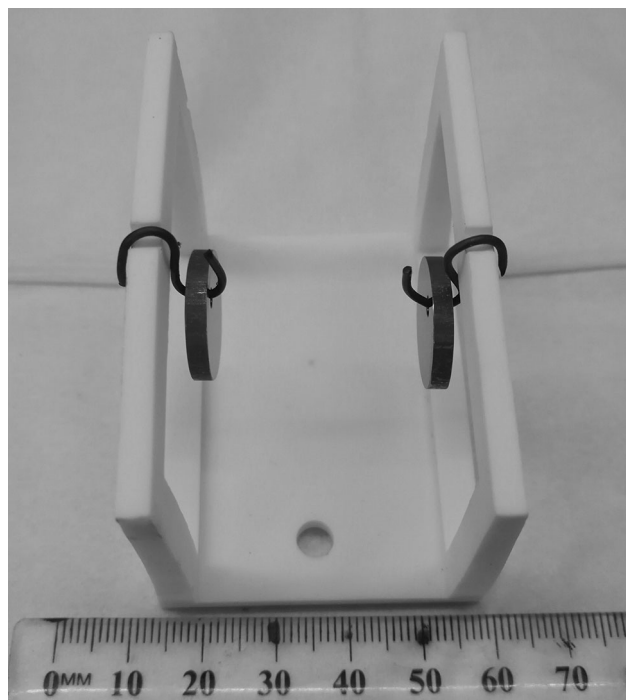| C	Si	Mn	P	S	Cr	Ni	Cu	Al
0.602	1.787	0.789	0.013	0.009	0.198	0.010	0.022	0.0038

Fig. 1—Experimental specimens suspended on an alumina stand in an experiment.

experiments. Two specimens were suspended in an alumina stand, as shown in Figure 1, in each experiment.

The experiments were conducted using a tube furnace. It is known that the moisture content in the atmosphere of a gas-fired furnace contains 15 to 25 pct of water vapor,[22] and therefore, 20 pctH$_2$O-N$_2$ was chosen to simulate the situation where no excessive air is used for combustion, which was obtained by flowing nitrogen through a water bath maintained at 60 °C.

In a typical experiment, the furnace was heated to the target temperature and allowed to stabilize. The alumina stand with the steel specimens suspended was then pushed slowly to the hot zone, while a protective 3 to 5 pct H$_2$-N$_2$ gas was flowing through the furnace chamber to prevent the specimens from oxidation. The specimens were preheated for 10 minutes in the H$_2$-N$_2$ gas to the target temperature and then the H$_2$-N$_2$ gas was switched to high purity nitrogen for 2 minutes to purge away the remaining H$_2$ gas. Thereafter, the nitrogen gas was switched to the 20 pct H$_2$O-N$_2$ gas, flowing at a rate of 3 liters per minute (L/min), equivalent to an average linear velocity of 1.3 cm/s at room temperature, or 5 to 6 cm/s at the reaction temperatures, to start the experiment. During each experiment, a thermocouple was inserted to the hot zone, located between two coupons, to monitor the reaction temperature, which was used to adjust the furnace setpoint if necessary. The thermocouple was calibrated using a Level 1 standard thermocouple. It was found that the measured temperatures were 1 °C to 3 °C below the readings of the standard thermocouple. During isothermal holding, the actual temperature was found to be increasing within 1 °C to 3 °C. Therefore, the quoted temperatures in the current study are considered to be accurate to ± 3 °C to 5 °C, unless some other unknown factors had affected the temperature readings.

After the completion of the experiment, the reaction gas was switched to high-purity nitrogen and then the specimens were retrieved to the cold zone of the furnace. After the specimens in the cold zone were cooled to a temperature below 300 °C, they were removed from the furnace and allowed to cool in air to room temperature. Repeated experiments were also conducted for the temperature range of 805 °C to 845 °C, within which decarburization was found to be very severe, at an interval of 10 °C.

To determine if there was any weight loss incurred during preheating, two specimens were retrieved to the cold zone immediately after preheating and allowed to cool in the cold zone to room temperature in the H$_2$-N$_2$ gas used. No weight loss was detected and the steel surface remained shining with no sign of oxidation.

After oxidation, the weight gains for all samples were measured and compared. These will be shown as apparent weight gains of the specimens. Without decarburization, the weight gains obtained can be used to convert to the scale thicknesses directly. However, as different degrees of decarburization occurred at different temperatures. By calculation, a depth of 100 μm complete decarburization zone is equivalent to a weight loss of 0.4716 mg/cm^2, as calculated below,

$$\text{Weight loss} = 0.602 \, \text{pct} \times 7.86 \text{ g/cm}^3 \times 0.01 \text{cm}$$
$$= 0.0004716 \text{ g/cm}^2 \quad [1]$$

where 0.602 pct is the carbon concentration of the steel, 7.86 g/cm^3 is the density of the steel and 0.01 cm = 100 μm is the thickness of the decarburization layer. It will be also shown that there will be different degrees of partial decarburization zone in the steel. The weight losses in the partial decarburization zone could not be measured accurately, and therefore, they were integrated from the carbon concentration profile for each temperature, which was calculated using conventional diffusion theories, as will be demonstrated later. The calculated weight losses due to complete and partial decarburization were then added to the measured weight gain to obtain the total weight gain for each temperature, which

was used to represent the actual scale thickness obtained due to oxidation.

All specimens were examined metallographically. After grinding and polishing following the usual procedure,[23] nital (4 pct nitric acid in methanol) was used to reveal the decarburization structures. The ferrite thicknesses as a result of decarburization were measured using the optical images taken at 200 times magnification. More details of the experimental methods can be found elsewhere.[24]

III. RESULTS

the apparent weight gains obtained within the range of 700 °C to 900 °C were very small as shown by the dotted line in Figure 2. After adding the weight losses due to decarburization, the total weight gains increased significantly for the range 750 °C to 900 °C (Figure 2). It is seen that the total weight gains from 780 °C to 900 °C were essentially unchanged, corresponding to a scale thickness of about 6 μm with those at 700 °C to 750 °C having a thickness of about 4 μm.

The cross-sections showing the decarburization depths and scales formed are shown in Figure 3. The measured thicknesses of the ferrite layers are plotted in Figure 4, as compared with theoretically calculated results. The methods of calculation to obtain the calculated results will be discussed in the Discussion section. Based on the findings of previous studies where the steels were oxidized in a H_2O-N_2 mixture[24] and confirmed by EDS, the thin-scale layers formed at all temperatures were wustite or primarily wustite. Consistent with the total weight gains shown in Figure 2, the scale thicknesses formed at different temperatures were similarly thin (4 to 6 μm if observed at higher magnifications, images not shown), whereas the thickness of the ferrite layers differed significantly.

After oxidation and decarburization at 700 °C, only a very thin ferrite layer (~ 5 μm) was observed, Figures 3(a) and 4. However, by increasing the temperature to 750 °C, this layer was increased to about 50 to 60 μm, Figures 3(b) and 4. A further increase of the temperature to 800 °C increased the ferrite layer thickness further by about 40 μm, Figures 3(c) and (d) and 4. The ferrite layer thickness reached its maximum of about 100 to 105 μm within the range of 805 °C to 825 °C, Figures 3(d) through (f) and 4, and then gradually decreased to about 30 μm at 900 °C, Figures 3(f) through (i) and 4. This ferrite thickness pattern as a function of temperature within 805 to 845 was confirmed by the results of the second set of experiments, Figure 4.

Adjacent to the ferrite layer formed, a partial decarburization zone was observed in the samples decarburized at 750 °C to 900 °C with its depth increasing with increased temperature, as seen in Figures 3(b) through (i). At 900 °C, it reached a depth of more than 200μm, Figure 3(i). This layer was absent at 700 °C, Figure 3(a).
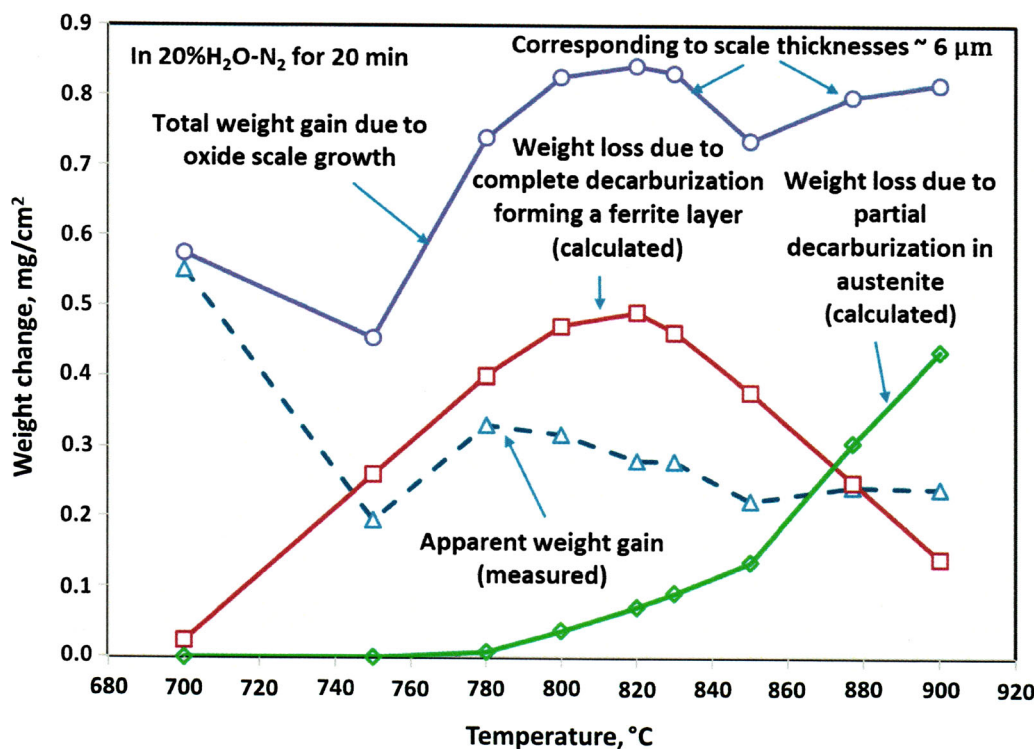

Fig. 2—Weight gain due to scale growth as a function of temperature. Apparent weight gains were obtained from measured weight gain data. Weight losses due to complete decarburization and partial decarburization were calculated, based on measured ferrite layer thicknesses and calculated partial decarburization profiles in austenite. Total weight gains were the sums of apparent weight gains and weight losses due to decarburization.

(a)

(b)

100 μm

(c)

(d)

(e)

(f)

Internal oxidation zone

Complete decarburization zone

Partial decarburization zone

(g)

(h)

(i)
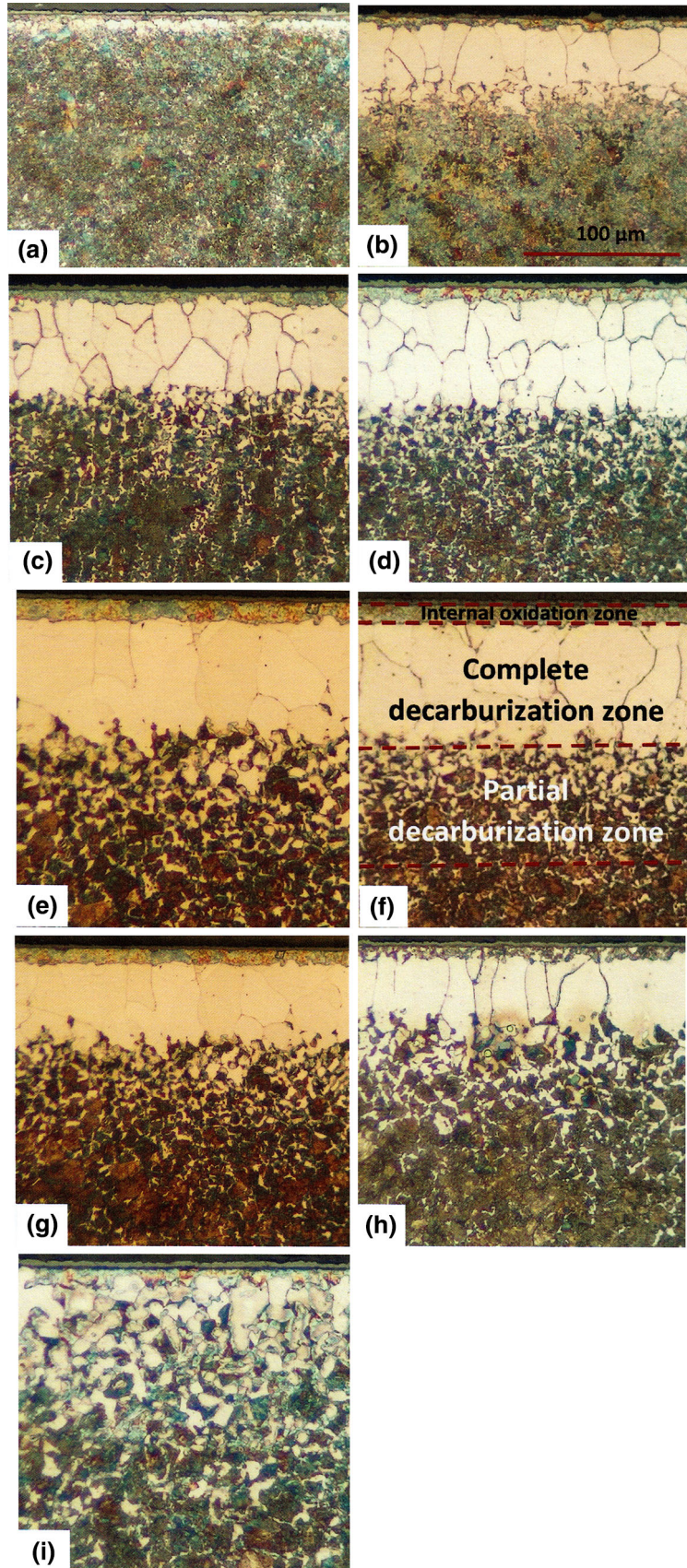
Fig. 3—Optical images of cross-sections of the specimens oxidized and decarburized at (*a*) 700 °C, (*b*) 750 °C, (*c*) 780 °C, (*d*) 800 °C, (*e*) 820 °C, (*f*) 830 °C, (*g*) 850 °C, (*h*) 877 °C and (*i*) 900 °C. Different zones in the specimens are labeled in (f). All images were taken at the same magnification of 200 times with a scale bar shown in (b).

An internal oxidation zone was also observed in the ferrite layer near the FeO-ferrite interface, as indicated in Figure 3(f), and shown more clearly in Figures 5 and 6. From the SEM image shown in Figure 6, it appeared that the internal oxides formed both inter-granularly along the original austenite grain boundaries as continuous layers (dark lines) and also intra-granularly as spherical precipitates. A significant amount of Si, together with iron and oxygen, was detected in the internal oxides. No further examination was conducted to obtain the actual compositions of the internal oxides, but the internal oxides observed were believed to be primarily SiO_2, as will be discussed later.

EDS analyses (not shown) found that there were no noticeable differences in the levels of Si, Mn and Cr in the ferrite layers and in the bulks of the steel samples, indicating that the movement of the ferrite–austenite interface was driven solely by carbon diffusion away from this interface.

IV. DISCUSSION

The possibility of forming a ferrite layer below 900 °C for Fe-C steel is well known.[18] This is because ferrite is stable under 912 °C and with the loss of carbon from the bulk of steel, the surface layer will transform to ferrite. For steels containing alloying elements, the critical temperature is different as some alloying elements, such as Si and Cr, stabilize ferrite and others, such as Mn and Ni, stabilize austenite. For the 60Si2MnA steel examined, two isopleths with constant concentrations of Si: 1.787 wt pct, Mn: 0.789 wt pct and Cr: 0.198 wt pct, were computed using Pandat[TM] software[25] and PanFe thermodynamic data base[26] as shown in Figure 7. It is seen that, in theory, a ferrite layer is able to form up to 950 °C and a layer of ferrite + austenite develops within 950 °C to 1020 °C if decarburization occurs to the steel.

It was claimed in the early studies[18–21] that when a ferrite layer formed, it would act as a diffusion barrier due to the very low solubility of carbon in ferrite, leading to a much reduced decarburization rate. However, recent studies[6–17] found that this was not the case. In an attempt to predict ferrite layer growth, Nomura *et al.*[6] used the equation derived by Wagner[27] and simplified by Smith,[28] to be named Wagner–Smith equation, to calculate the ferrite layer thicknesses at 700 °C and 850 °C to 950 °C for several spring steels and found peak values at 850 °C. The calculated results for
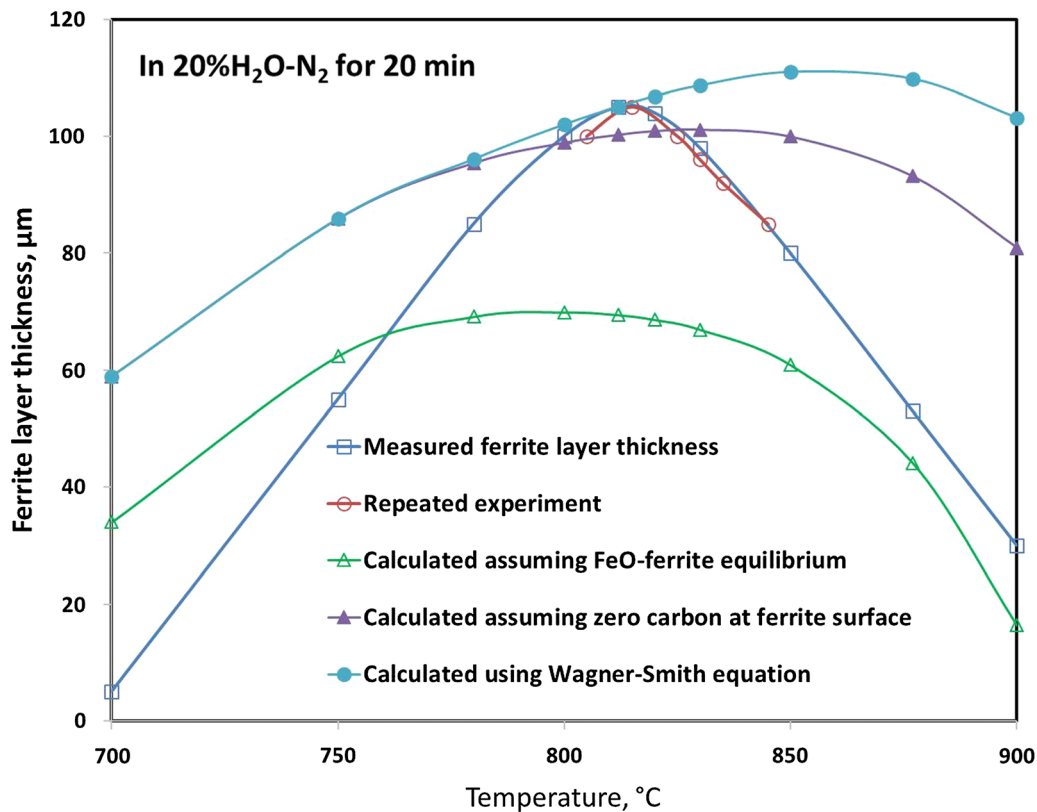
Fig. 4—Comparison of measured ferrite layer thickness as a function of decarburization temperature, and those calculated using different methods.
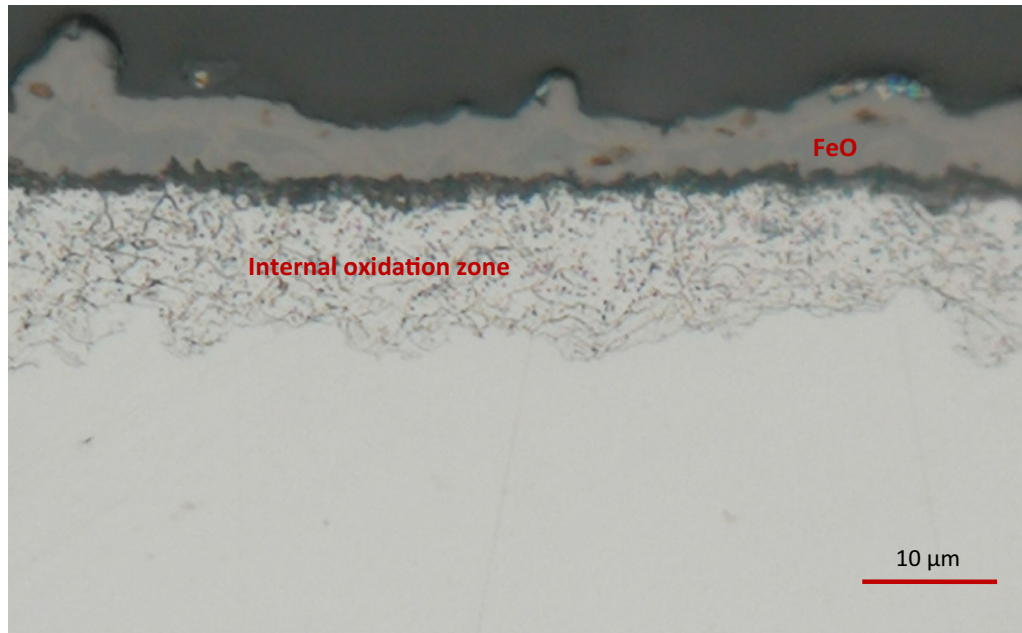
Fig. 5—Optical image of the oxide scale layer and internal oxidation zone in the sample oxidized at 835 °C for 20 min.
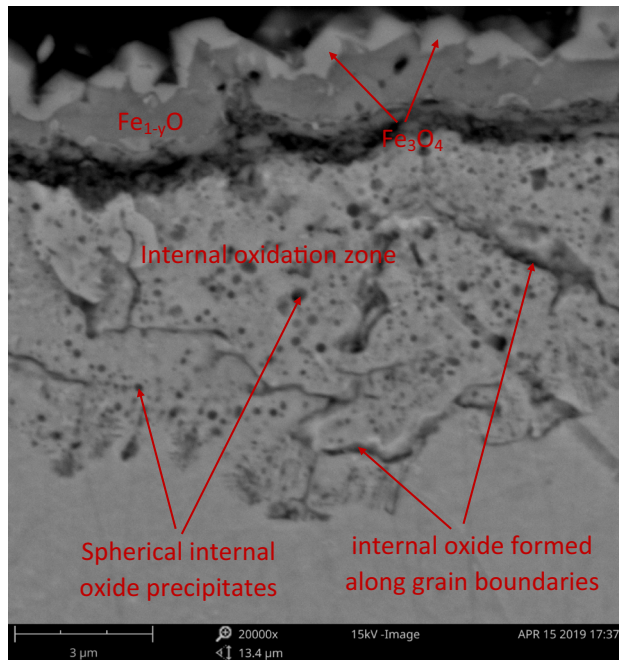

Fig. 6—SEM image of the oxide scale layer and internal oxidation zone in the sample oxidized at 835 °C for 10 min. A significant amount of Si, together with iron and oxygen, was detected in the internal oxides.

the range of 700 °C to 850 °C were not presented and no experimental results were obtained for this range. It was also noticed that the Wagner–Smith Equation used by Nomura et al. was derived under the assumption that the carbon concentration at the steel surface was zero, and in the calculation, the data used for carbon diffusion in ferrite was obtained from the equation for much lower temperatures (− 40 °C to 350 °C),[29] which was known to be unsuitable for predicting higher temperature diffusivities. It was also noted that carbon diffusion in austenite was not taken into consideration in their prediction. In view of these, new methods need to be developed for better predictions of spring steel decarburization.

It was demonstrated in a recent study that dissolved carbon in steel was able to react with wustite formed on steel, leading to simultaneous reduction of the wustite scale and decarburization of the steel substrate.[30] The scale layer formed in the current study was found to comprise wustite (FeO) only, or primarily wustite, with the wustite phase in contact with the steel. The wustite phase would then be able to react with the dissolved carbon in the steel, leading to decarburization. If this occurred, then the carbon concentration at the scale–steel interface would be determined by the equilibrium reactions taking place between FeO and dissolved carbon in the steel. A permeability concept was then developed in the recent study[30] to explain the observed oxide scale reduction kinetics by dissolved carbon in the steel with a good success.

In the current study, we will first use the permeability approach developed in the previous study[30] to assess the decarburization tendency, and then a more rigorous approach using the original equations derived by Wagner[27] will be used to calculate the ferrite layer thicknesses under both the assumptions of zero carbon concentration and FeO-ferrite equilibrium at the steel surface. The calculated results will be compared with experimental results and the results calculated from the Wagner–Smith equation used by Nomura et al.[6]

From Figure 7,[25,26] it can be seen that at temperatures below 774 °C, the bulk of steel is in either a two-phase bcc–fcc (ferrite-austenite), three-phase
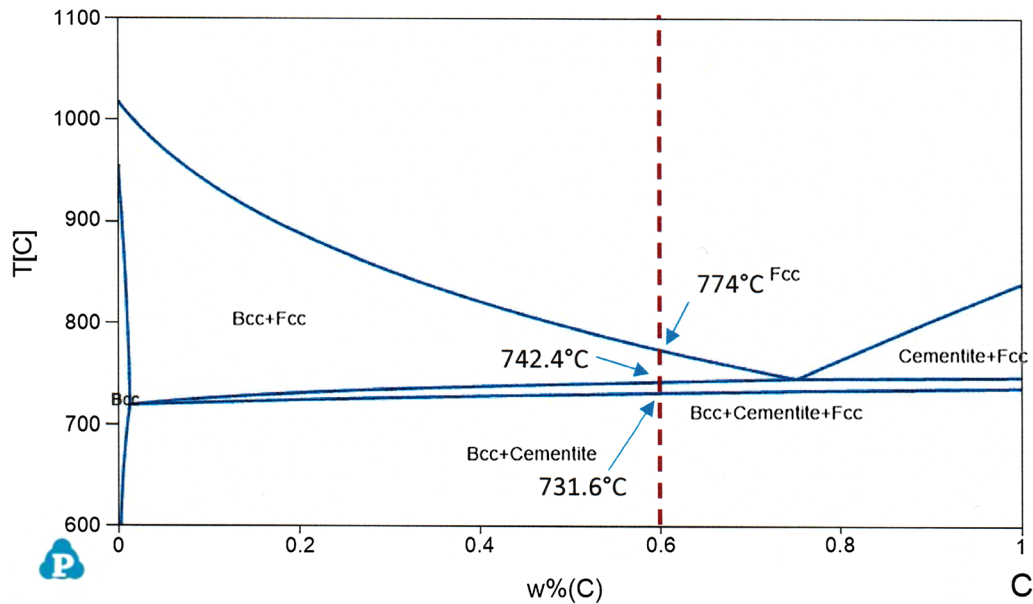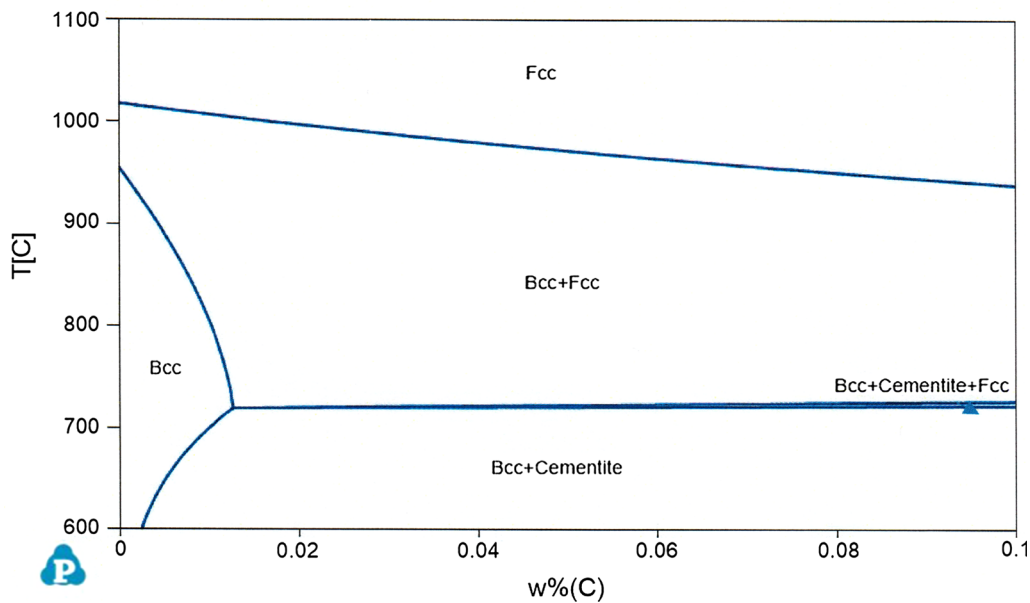
Fig. 7—Fe-C isopleths at 1.787 wt pct Si-0.789 pct Mn-0.198 pct Cr for the range of (*a*) 0 to 1 wt pct C and (*b*) 0 to 0.1 wt pct C, calculated using Pandat[TM].[25, 26]

bcc-fcc-Fe$_3$C (ferrite-austenite-cementite) or a two-phase bcc-Fe$_3$C state. In this case, the carbon concentration in the ferrite phase at the ferrite/bulk interface is considered to be equal to that in the ferrite phase in the bulk of steel, and the growth of ferrite layer takes place at the expense of the bulk of the steel, as schematically illustrated in Figure 8.

At temperatures above 774 °C, on the other hand, the bulk of steel was in a single-phase austenitic state. With the loss of carbon and the formation of a ferrite layer on the surface, a carbon concentration gradient would develop at the region adjacent to the ferrite layer, as illustrated in Figure 9. Carbon diffusion in the austenite phase towards the ferrite–austenite interface would affect the growth of the ferrite layer, as it offsets the loss of carbon at the ferrite-FeO interface. As no redistributions of alloying elements were detected, the growth of ferrite layer was considered to be controlled by carbon diffusions only, under the para-equilibrium conditions maintained at the α–γ interface. Due to the inevitable formation of internal oxides, the alloying effect was considered to be negligible when the carbon concentration at the ferrite-FeO was calculated.
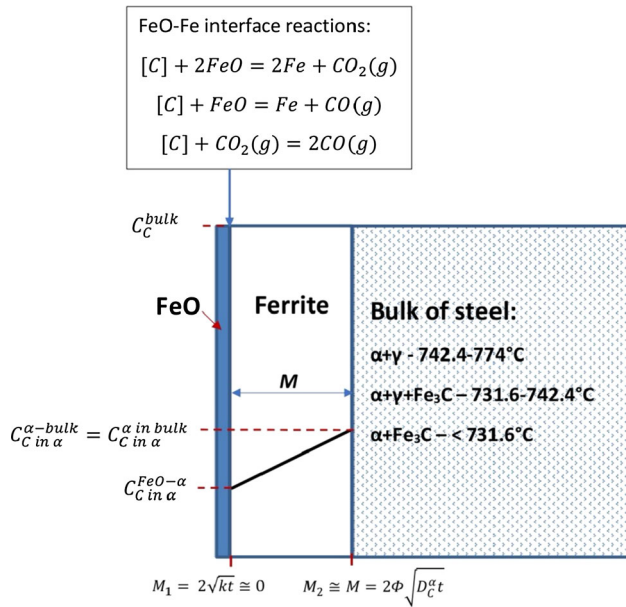
Fig. 8—Decarburization at T < 774 °C. The steel was in a two-phase α-Fe + γ-Fe state at 742.4 °C to 774 °C, two-phase α-Fe + Fe₃C state at T<731.6 °C and three-phase α-Fe + γ-Fe + Fe₃C state at 731.6 °C to 742.4 °C, based on the results obtained by Pandat$^{TM[25,26]}$ assuming no re-distribution of the alloying elements (Si, Mn and Cr) during ferrite growth. The carbon concentration in the bulk equals to the original carbon concentration $C_C^{bulk} = 0.602$ wt pct. Carbon concentration in ferrite at the ferrite–bulk interface is assumed to be equal to the carbon concentration of the α-Fe phase in the bulk. The carbon concentration in ferrite at the FeO-ferrite phase is determined by the simultaneous equilibria of the interface reactions indicated.

1. Carbon permeability through the ferrite layer

Following the procedure developed previously,[30] as detailed in Appendix I, the carbon flux diffusing through the ferrite layer J_C^α is expressed by the following equation,

$$J_C^\alpha = A \cdot \frac{P_C^\alpha}{M} \text{moles cm}^{-2}\text{s}^{-1} \qquad [2]$$

where A is a constant used to convert the carbon concentration from wt pct to mole/cm³, M the thickness of the ferrite layer and P_C^α the carbon permeability through the ferrite layer, defined as,

$$P_C^\alpha = D_C^\alpha \cdot (C_{Cin\alpha}^{\alpha-bulk} - C_{Cin\alpha}^{FeO-\alpha}) = D_C^\alpha \cdot \Delta C_C^\alpha \qquad [3]$$

with D_C^α being the diffusion coefficient of carbon in ferrite in cm²·s⁻¹, $C_{Cin\alpha}^{\alpha-bulk}$, in wt pct, the carbon concentration in the ferrite phase at the interface between the ferrite phase and the bulk of steel, as shown in Figure 8, and $C_{Cin\alpha}^{FeO-\alpha}$ the carbon concentration in ferrite at the FeO–ferrite interface in wt pct. When the bulk of steel is in an austenitic state, $C_{Cin\alpha}^{\alpha-bulk} = C_{Cin\alpha}^{\alpha-\gamma}$, with $C_{Cin\alpha}^{\alpha-\gamma}$ being the carbon concentration in the ferrite phase at the $\alpha - \gamma$ interface as shown in Figure 9.

It can be seen from Eq. [2] that for a given thickness of the ferrite layer, the carbon flux is proportional to the carbon permeability, and from Eq. [3], the carbon permeability is a function of two variables, carbon
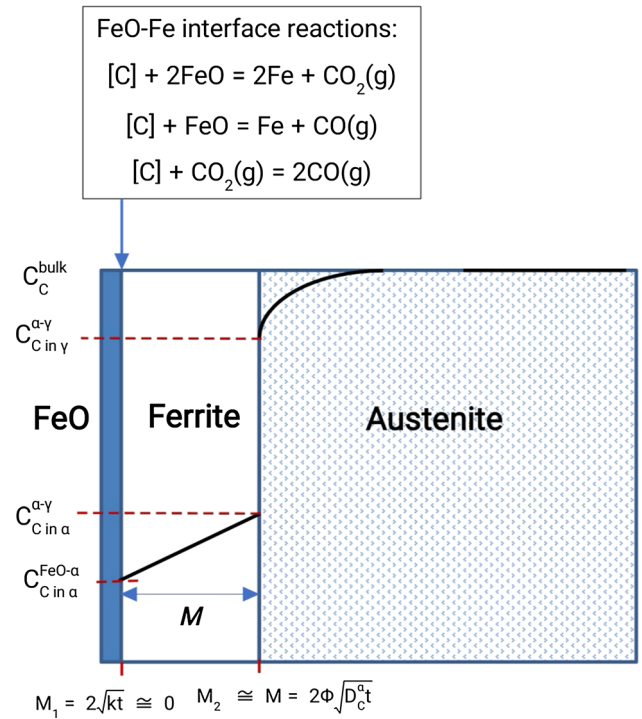

Fig. 9—Decarburization at T > 774 °C. The carbon concentration in the bulk equals to the original carbon concentration, $C_C^{bulk} = 0.602$ wt pct. Carbon concentrations in austenite and ferrite at the $\alpha-\gamma$ interface, $C_{Cin\gamma}^{\alpha-\gamma}$ and $C_{Cin\alpha}^{\alpha-\gamma}$, are determined by the para-equilibrium between the two phases, assuming no re-distribution of the alloying elements (Si, Mn and Cr) with the carbon activities maintaining equal during the decarburization process. Carbon concentration in ferrite at the FeO-ferrite interphase is determined by the simultaneous equilibria of the interface reactions indicated.

diffusivity in ferrite and the concentration difference at its two interfaces. Strictly speaking, the driving force for carbon diffusion through the ferrite layer is the chemical potential difference at the two interfaces. However, under the assumption of constant concentrations of the alloying elements (Si, Mn and Cr), the chemical potential difference is equivalent to the carbon concentration difference.

From Figure 7(b), it can be seen that the saturated carbon concentration in ferrite (at the inner interface of the ferrite layer shown in Figures 8 and 9) reaches its maximum at 715 °C, as plotted more clearly in Figure 10(a). If the carbon concentration at the surface of the ferrite layer is assumed to be zero, then the driving force (carbon concentration difference) for diffusion through the ferrite layer reaches its maximum at 715 °C.

However, as the steel surface was in contact with a wustite scale, it was more likely that the carbon concentration at the steel surface, or FeO-ferrite interface, was determined by the reaction equilibria indicated in Figures 8 and 9, which was found to decrease with increased temperature, as shown in Figure 10(a). Therefore, the carbon concentration difference between the two interfaces were different from that determined by the saturated carbon concentration in ferrite only, becoming nearly unchanged within the range of 715
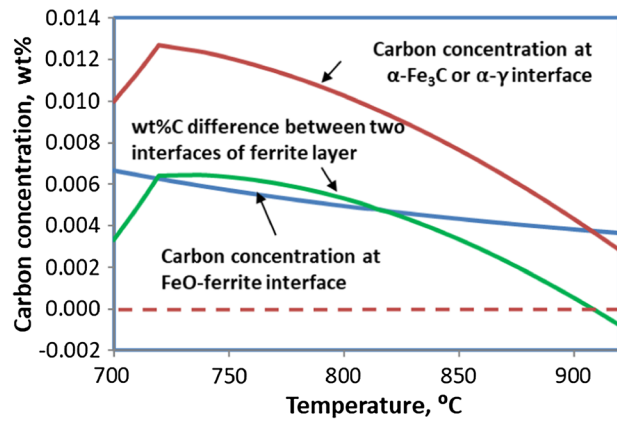
(a)
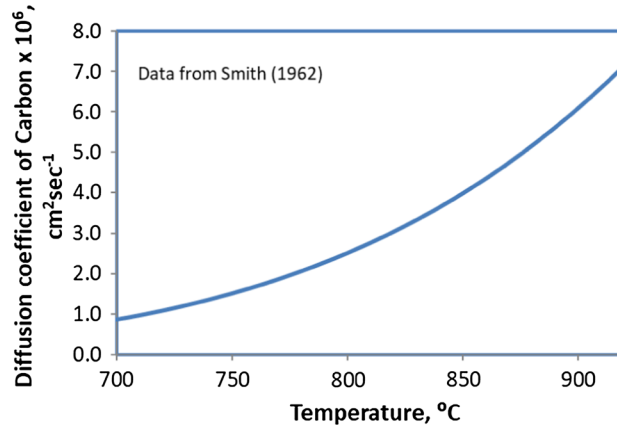
(b)
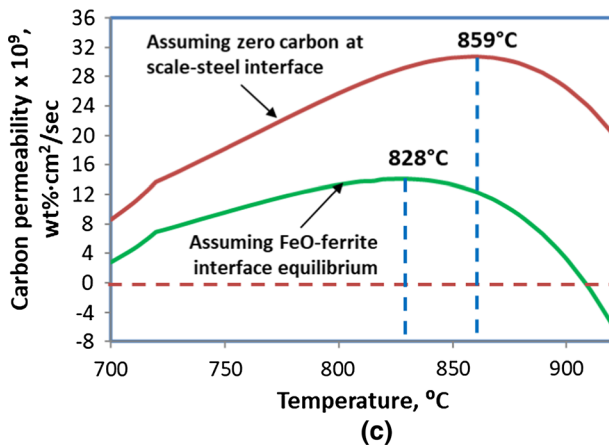
(c)

Fig. 10—Determination of carbon permeabilities under two different scale–ferrite interface conditions (FeO-ferrite equilibrium and zero carbon at steel surface): (*a*) carbon concentration differences at the two interfaces of the ferrite layer, (*b*) carbon diffusivity in ferrite (data from Smith 1962[28]) and (*c*) calculated carbon permeabilities.

°C to 750 °C, Figure 10(a). Using the diffusivity data in ferrite given by Smith[28], which was found to increase monotonically and exponentially with increased temperature as shown in Figure 10(b), and the carbon concentration differences under the two assumed carbon concentrations at the FeO-ferrite interfaces, the carbon

permeabilities were calculated and compared in Figure 10(c). It is seen that, under the assumption of zero carbon concentration at the steel surface, the carbon permeability reaches its maximum at 859 °C and within the temperature range of 860 °C to 920 °C, the carbon permeability remains very high, whereas, under the assumption of FeO-ferrite equilibrium, the calculated carbon permeability reaches its maximum at 828 °C, and more importantly, the calculated permeability decreases rapidly thereafter towards 920 °C.

Clearly, as compared to the experimental results shown in Figure 4, the calculated permeability results under the FeO-ferrite equilibrium assumption showed a good match to the pattern of measured ferrite thickness change with temperature, where the ferrite layer thickness was observed to reach its maximum at 805 °C to 825 °C and became very small at 900 °C.

In contrast, the calculated permeabilities under the assumption of zero carbon at the ferrite surface showed very large discrepancies from the experimental data, with a much higher peak permeability temperature (859 °C) and much greater calculated permeabilities at temperatures near 900 °C.

Based on these results, it can be concluded that the surface carbon concentration was more likely determined by the interface reaction equilibrium between dissolved carbon in the ferrite phase and the FeO scale, similar to the observation made previously[30].

More importantly, the carbon permeability analyses, confirmed by experimental results, clearly demonstrated that severe decarburization could occur with the formation of a thick ferrite layer at a temperature well below 900 °C, due to the combined effect of two factors. First, there was a maximum carbon solubility in the ferrite phase, which provided a good driving force for the ferrite layer to grow, and second, the greater diffusivity in ferrite promoted rapid growth of the ferrite layer.

2. Calculation of ferrite layer growth at T < 774 °C

At T < 774 °C, with the loss of carbon from the steel, a ferrite layer would form when the carbon concentration was sufficiently low, but the steel substrate underneath would retain a two-phase or three-phase structure, as shown in Figure 7(a). In this case, the growth of the ferrite layer would be solely determined by carbon diffusion through the ferrite layer.

As the scale thickness observed was small (≤ 6 μm), in calculating the ferrite growth in the current study, the scale-ferrite interface was assumed to be stationery, *i.e.,* scale growth was negligible, during the decarburization process, as shown in Figure 8. The original equation derived by Wagner[27] to show the carbon concentration as a function of the distance through the ferrite layer and time had the following form,

$$C_{Cin\alpha} = C_{Cin\alpha}^{FeO-\alpha} + \frac{C_{Cin\alpha}^{\alpha-bulk} - C_{Cin\alpha}^{FeO-\alpha}}{erf(\Phi)} erf\left(\frac{x}{2\sqrt{D_C^{\alpha}t}}\right) \quad [4]$$

where Φ is a constant value at a given temperature, determined by the following relationship:

$$F(\Phi) = \sqrt{\pi} \times \left(C_C^{bulk} - C_{Cin\alpha}^{\alpha inbulk} \right) - \frac{C_{Cin\alpha}^{\alpha inbulk} - C_{Cin\alpha}^{FeO-\alpha}}{\Phi e^{\Phi^2} \text{erf}(\Phi)} = 0$$

$$[5]$$

Once the Φ is found, the ferrite layer thickness, M, can be calculated using the following equation,

$$M \cong M_2 = 2\Phi\sqrt{D_C^\alpha t} \qquad [6]$$

where M_2 is the distance of the ferrite–austenite interface from the original steel surface, as defined in Figure 8.

3. Calculation of ferrite layer growth at T > 774 °C

At T > 774 °C, however, with the formation of a ferrite layer on the steel surface, the steel bulk underneath would be in an austenitic state where a carbon concentration gradient would be established, as shown in Figure 9. Supply of carbon in the austenite phase by diffusion to the ferrite–austenite interface would affect the growth of the ferrite layer, and therefore, must be taken into account when calculating the growth of the ferrite layer.

As the boundary conditions for the growth of the ferrite layer are the same at all temperatures, regardless of whether carbon diffusion in the austenite contributed to the ferrite growth or not, the carbon concentration in the ferrite layer can still be described by Eq. [4] but takes the form of,

$$C_{Cin\alpha} = C_{Cin\alpha}^{FeO-\alpha} + \frac{C_{Cin\alpha}^{\alpha-\gamma} - C_{Cin\alpha}^{FeO-\alpha}}{\text{erf}(\Phi)} \text{erf}\left(\frac{x}{2\sqrt{D_C^\alpha t}} \right) \quad [7]$$

Following the procedure given by Wagner[27] and using the initial condition at $t = 0$ and $x \geq 0$, or $\eta = \frac{x}{2\sqrt{D_C^\gamma t}} = \infty$, $\text{erfc}(\eta) = 0$ and $C_{Cin\gamma} = C_{Cin\gamma}^{bulk} = 0.602$ wt pct, and the boundary condition at $x = M \cong M_2 = 2\Phi\sqrt{D_C^\alpha t}$, $C_{Cin\gamma} = C_{Cin\gamma}^{\alpha-\gamma}$, the carbon concentration in austenite as a function of distance and time can be obtained:

$$C_{Cin\gamma} = C_{Cin\gamma}^{bulk} + \frac{C_{Cin\gamma}^{\alpha-\gamma} - C_{Cin\gamma}^{bulk}}{\text{erfc}\left(\cdot\frac{\Phi}{\beta} \right)} \text{erfc}\left(\frac{x}{2\sqrt{D_C^\gamma t}} \right) \quad [8]$$

where D_C^γ is the carbon diffusivity in austenite, in cm^2/s, and the constant β is defined as,

$$\beta = \frac{\sqrt{D_C^\gamma}}{\sqrt{D_C^\alpha}} \qquad [9]$$

The Φ value in Eq. [8] can be obtained by solving the following equation, which was derived by considering mass balance at the α–γ interface,

$$F(\Phi) = \sqrt{\pi} \cdot \left(C_{Cin\gamma}^{\alpha-\gamma} - C_{Cin\alpha}^{\alpha-\gamma} \right)$$
$$- \left[\frac{C_{Cin\gamma}^{\alpha-\gamma} - C_{Cin\gamma}^{bulk}}{\frac{\Phi}{\beta} \cdot e^{\left(\frac{\Phi}{\beta}\right)^2} \cdot \text{erfc}\left(\frac{\Phi}{\beta}\right)} + \frac{C_{Cin\alpha}^{\alpha-\gamma} - C_{Cin\alpha}^{FeO-\alpha}}{\Phi \cdot e^{\Phi^2} \cdot \text{erf}(\Phi)} \right]$$
$$= 0 \qquad [10]$$

The Φ value thus obtained can then be used to calculate the thickness of the ferrite layer thickness using Eq. [6].

The calculated ferrite thickness under two different assumptions, i.e., $C_{Cin\alpha}^{FeO-\alpha}$ determined by FeO-ferrite equilibrium and $C_{Cin\alpha}^{FeO-\alpha} = 0$, are plotted in Figure 4, where the results calculated using the Wagner–Smith equation used by Nomura et al.,[6, 28]

$$M = \sqrt{\frac{6 \cdot C_{Cin\alpha}^{\alpha-\gamma} \cdot D_C^\alpha \cdot t}{3 \cdot C_C^{bulk} - 2 \cdot C_\alpha^{\alpha-\gamma}}} \qquad [11]$$

where $C_C^{bulk} = 0.602$ wt pct is the initial carbon concentration of the steel, are also presented, as compared to the experimental data.

It can be seen from these results that when the carbon concentration was assumed to be zero, although the calculated ferrite layer thickness matched the experimental data at 800 °C to 820 °C, the calculated thicknesses at the lower and higher temperature ranges deviated drastically from experimental results. In particular, the calculated ferrite thicknesses at temperatures close to 900 °C were very high when the original Wagner's equations Eqs. [4 through 10] was used. They were even higher when the Wagner–Smith equation, Eq. [11], was used. This was because when Eq. [11] was used, it was not only assumed that the carbon concentration at the steel surface was zero, but it was also assumed that carbon diffusion in the austenite phase at temperatures above 774 °C did not affect the growth of the ferrite phase and at the same time, the carbon concentration at the ferrite-austenite interface was assumed to be equal to the bulk concentration.

On the other hand, when the carbon concentration at the scale–ferrite interface was assumed to be determined by the FeO-ferrite equilibrium and the diffusion of carbon in austenite was taken into account, the calculated ferrite layer thicknesses showed a thickness pattern closer to that of the experimental results. In particular, the calculated ferrite layer thicknesses for the temperature range near 900 °C were very close to experimentally observed values (Figure 4). However, given the large discrepancy between the calculated ferrite layer thicknesses and those observed at the 780 °C to 840 °C, the method used cannot be considered to be a complete success. Other factors, such as the actual diffusivities of carbon in both ferrite and austenite, and the actual carbon concentrations in ferrite and austenite at the α–γ interface during ferrite growth, and the alloying effects should be considered in future studies. Alternatively, it

could be possible that the FeO-ferrite interface condition was different at different temperature ranges with the values at about 780 °C to 840 °C being zero carbon, those near 900 °C being controlled by FeO-steel equilibrium, and those at 700 °C to 750 °C being greater than the FeO-ferrite equilibrium values.

Previous studies found that the diffusivity of carbon in austenite was a function of carbon concentration[31–35] and affected significantly by the presence of alloying elements.[36–43] Fewer experimental studies were conducted[29,36,44–48] to address the effect of carbon concentration and alloying elements on the diffusivity of carbon in ferrite. In the current study, the diffusivities in unalloyed ferrite obtained by Smith[28] and the equation derived by Lee et al. for alloyed austenite[38] were used for calculation, but in the latter, the carbon concentrations in austenite at the α-γ boundary were used. An attempt was made to use the diffusivities given by Lord and Beshers[44] for calculation, but the resulting ferrite thicknesses were much smaller than experimental results and therefore considered to be unacceptable.

The saturated carbon concentration in ferrite (in equilibrium with austenite at T > 774 °C or with the bulk of steel at T < 774 °C) were obtained from the calculated isopleth data, which were computed under complete equilibrium conditions between ferrite and austenite[26]. In the real situation, the saturated carbon concentrations in ferrite at the α–γ (T > 774 °C) would be different from the data used, determined by a condition close to para-equilibrium between the two phases.[49, 50] Future studies will assess more details of various factors that could affect the predicted results.

4. Partial decarburization in austenite

Partial decarburization in the ferrite phase was clearly observed at 780 °C to 900 °C with the depth at 900 °C being the greatest, exceeding 200 μm. The carbon profiles in the partial decarburization zones at these temperatures were calculated using Eq. [8] and shown in Figure 11. No attempt was made to measure the carbon concentration gradient in the austenite phase in the current study, but by comparing with the images shown in Figure 3, the depth of partial decarburization zone did show a deepening pattern with increased temperature, as predicted in Figure 11.
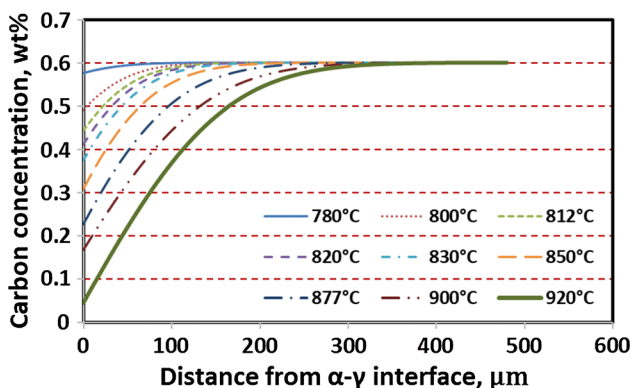

Fig. 11—Partial decarburization in austenite (calculated).

5. Internal oxidation

An internal oxidation layer was observed in the ferrite layer at all temperatures (Figures 3, 5 and 6). SEM observations (Figure 6) found that the internal oxides had two forms, spherical precipitates or line precipitates. The presence of much higher levels of silicon in the internal oxides than in the steel was confirmed by EDS analyses (results not shown). These morphologies were similar to those observed by Takada and Adachi[51], who used the XRD method to analyze extracted internal oxides formed in Fe-Si alloys but found no diffraction peaks, suggesting that they were amorphous.

Li et al. recently studied the oxidation behavior of Fe-1 to 3 wt pct Si alloys in dry and wet CO_2 gasses at 800 °C[52, 53] and found that the internal oxides were presented in two forms, rod-shaped precipitates (in 1 wt pct Si-Fe) and also developed into a network pattern (in 3 wt pct Si-Fe). From XRD, EDS and selected area diffraction (SAD) analyses, it was concluded that the internal silicon oxide was amorphous SiO_2.

Using an organic solvent, Kusabiraki et al.[54,55] found that amorphous SiO_2 formed inter and intra-granularly in Fe-Si alloys after oxidation at 1100 °C to 1200 °C in flowing air or a furnace atmosphere containing 17 pct H_2O-8 pct CO_2-1 pct O_2 and the SiO_2 phase formed along grain boundaries as wall-like films.

Given the similarity of the morphologies observed to those observed by others, it was believed that the internal oxides were most likely to be amorphous SiO_2. More detailed examination of the formation of these oxides was outside the scope of the current study.

Formation of internal oxides would consume silicon from the steel surface layer, and therefore, decrease the level of silicon in solution in ferrite near the scale–steel interface. With the decreased silicon level, the carbon activity in the surface layer would be decreased for a given carbon concentration and hence the carbon activity difference between the two interfaces of the ferrite layer would be also increased. In this way, the rate of decarburization would be increased. This could provide an explanation of why the presence of silicon in steel would make the steel more susceptible to decarburization. However, it seemed unable to provide an explanation for the discrepancy between the calculated and observed ferrite layer thicknesses at 780 °C to 840 °C because internal oxidation was observed at all the temperatures examined.

V. CONCLUSIONS

The decarburization behavior of a commercial spring steel 60Si2MnA at 700 °C to 900 °C in 20 pct H_2O-N_2 was studied experimentally and theoretically, leading to the following conclusions.

1. It was observed experimentally that after 20 minutes of holding in 20 pct H_2O-N_2, a thick ferrite layer developed on the steel surface at the temperature range of 750 °C to 880 °C with the maximum thickness of 100 to 105 μm observed at 805 °C to

825 °C, but at 700 °C and 900 °C, the thicknesses of the ferrite layer were very small ($< 30 \mu$m).

2. The development of a ferrite layer was analyzed using existing diffusion theories. Using the permeability concept and under the assumption of FeO-ferrite equilibrium, the pattern of thickness change with temperature could be qualitatively and successfully determined.

3. The ferrite layer thicknesses were also calculated using existing diffusion theories and available experimental data. When the carbon concentration at the scale-steel interface was assumed to be zero, the calculated ferrite layer thicknesses matched the experimental results well only at 800 °C to 820 °C, but the calculated results for the lower and higher temperature ranges deviated drastically from experimental results.

4. When the carbon concentration at the steel surface was assumed to be determined by reaction equilibrium between wustite and dissolved carbon in steel, the calculated pattern of ferrite layer thickness change with temperature had a better match with experimental results, and the calculated small ferrite thicknesses near 900 °C were particularly encouraging. However, the calculated maximum ferrite layer thickness at 780 °C to 840 °C could not match the observed values well. Factors that could have contributed to the discrepancy were discussed.

5. Partial decarburization was observed underneath the ferrite layer, with the severity increasing with temperature. The calculated partial decarburization profiles in the austenite compared qualitatively well with observed results.

6. Internal oxidation occurred to the steel and the morphologies shown were consistent with those observed by others. Formation of internal SiO_2 would consume silicon in solution in the surface layer of the steel, thus lowering the carbon activity near the FeO-ferrite interface and hence accelerating decarburization. This could provide an explanation of why the presence of silicon in steel increased the susceptibility of the steel towards decarburization.

APPENDIX I: DETERMINATION OF THE CARBON PERMEABILITY THROUGH THE FERRITE LAYER[30]:

In determining the equilibrium carbon concentration at the scale–steel interface, it is assumed that the dissolved carbon in steel can react with wustite, forming either CO and CO_2 via the following reactions:

$$[C] + 2FeO = 2Fe + CO_2 \qquad [A1]$$

$$[C] + FeO = Fe + CO \qquad [A2]$$
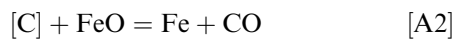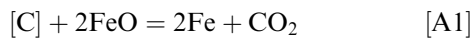
and the overall reaction of these reactions becomes:

$$CO + FeO = Fe + CO_2 \qquad [A3]$$
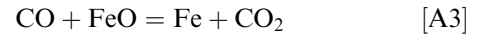
Using the data given by Richardson and Jeffes[56] and quoted by Kubaschewski and Alcock,[57] the standard Gibbs free energy of formation for Reaction (A3) is given by

$$\Delta G_{A3}^o = -22800 + 24.267T (J/\text{mole of CO}) \qquad [A4]$$

When the reaction (A3) reaches equilibrium,

$$\frac{P_{CO}}{P_{CO_2}} = \exp\left(\frac{-22800 + 24.267T}{RT}\right) \qquad [A5]$$

The $\frac{P_{CO}}{P_{CO_2}}$ thus obtained can be used to determine the equilibrium carbon activity at the interface assuming $P_{CO} + P_{CO_2} = 1$ atm from the following reaction:

$$[C] + CO_2(g) = 2CO(g) \qquad [A6]$$
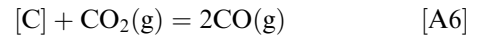
The standard Gibbs free energy of formation for this reaction is given by,[56,57]

$$\begin{aligned}\Delta G_{A6}^o &= -RT \ln\left[\frac{P_{CO}^2}{a_c P_{CO_2}}\right] \\ &= 170,700 - 174.5T \, (J/\text{mole of C}) \qquad [A7]\end{aligned}$$

where a_c is the equilibrium activity of carbon at the scale-steel interface with graphite being its standard state. From Eq. [A7], we obtain,

$$a_c = \frac{P_{CO}^2}{P_{CO_2}} \exp\left[\frac{(170,700 - 174.5T)}{RT}\right] \qquad [A8]$$

After the equilibrium carbon activity at the interface is determined, the corresponding carbon concentration in the steel at the scale-steel interface can be calculated using the known relationships between carbon activities and carbon concentrations. For dissolved carbon in α-Fe, the relationship to express the activity coefficient of carbon in ferrite for carbon steel, $\Upsilon_C(\text{ferrite})$, is given by,[58]

$$\log \Upsilon_C(\text{ferrite}) = \log\left(\frac{a_C}{X_C}\right)(\text{ferrite}) = \frac{5846}{T(K)} - 2.687 \qquad [A9]$$

where X_C is the equilibrium molar fraction of carbon in ferrite at the scale-steel interface, which can be converted to carbon concentration in weight percent using the following equation,

$$C_c(\text{wt pct}) = \frac{100 \, \text{pct} \cdot 12 \cdot X_c}{12 \cdot X_c + 55.85 \cdot (1 - X_C)} \qquad [A10]$$

When a ferrite layer formed on the steel surface and the alloy concentrations are constants across the ferrite layer, the difference in the carbon concentration between two interfaces of the ferrite layer, ΔC_C^α, provides a

driving force for carbon to diffuse through the ferrite layer.

When the ferrite layer is thin, the carbon distribution in it can be approximated as having a linear concentration gradient and carbon diffusion through this layer can be described using the simplified Fick's first law:

$$J_C^\alpha = A \cdot D_C^\alpha \cdot \frac{C_{Cin\alpha}^{\alpha-\gamma} - C_{Cin\alpha}^{\alpha-FeO}}{M} \text{ moles cm}^{-2}\text{s}^{-1} \quad [A11]$$

where J_C^α = the diffusion flux of carbon from the interface between the ferrite layer and the bulk of steel towards the scale-steel interface; D_C^α = the diffusion coefficient of carbon in ferrite; $C_{Cin\alpha}^{\alpha-\gamma}$ = the carbon concentration on the ferrite side at the interface between the ferrite layer and the bulk of steel in wt pct ; $C_{Cin\alpha}^{\alpha-FeO}$ = the carbon concentration in ferrite at the steel-scale interface in wt pct ; A = a constant used to convert the concentration of carbon from wt pct to mole/cm^3; M = the thickness of the ferrite layer.

From Eq. [A11], we can see that for a certain thickness of the ferrite layer, X, the rate of carbon diffusion is determined by the product of carbon diffusivity D_C^α and the carbon concentration difference between the two interfaces of the ferrite layer, $\Delta C_C^\alpha = C_{Cin\alpha}^{\alpha-\gamma} - C_{Cin\alpha}^{\alpha-FeO}$. Following the approach used by Smith,[28] the following product was defined as the *permeability or relative permeability*,[59] (P_C^α) *of carbon* through the ferrite layer,

$$P_C^\alpha = D_C^\alpha \cdot (C_{Cin\alpha}^{\alpha-\gamma} - C_{Cin\alpha}^{\alpha-FeO}) = D_C^\alpha \cdot \Delta C_C^\alpha \quad [A12]$$

Substitution of Eq. [A12] in Eq. [A11] yields,

$$J_C^\alpha = A \cdot \frac{P_C^\alpha}{M} \text{ moles cm}^{-2}\text{s}^{-1} \quad [A13]$$

It can be seen that a greater permeability immediately leads to a greater carbon flux for a given ferrite layer thickness.

Strictly speaking, the alloying effect, particularly the effect of Si, should be considered in calculating the carbon concentration from the carbon activity data obtained from Eq. [A8]. However, as internal oxidation was inevitably observed, it was assumed that the dissolved alloying components (Si, Mn and Cr) had reacted with dissolved oxygen having diffused into the steel and therefore, the alloying effect from the remaining dissolved alloying components at the FeO-steel interface was considered to be negligible.

REFERENCES

1. GB/T 1222 – 2016. Spring Steels, National Standards of the People's Republic of China (2016).
2. Designation: A29/A29M – 05. Standard specification for steel bars, carbon and alloy, hot-wrought, general requirement for. ASTM International (2006).
3. BS EN 10089:2002. Hot rolled steels for quenched and tempered springs – Technical delivery conditions, BSi British Standards (2002).
4. A.S. Kenneford: *J. Iron Steel Inst.*, 1950, vol. 164, pp. 265–77.
5. M.J. Geldersleeve: *Mater. Sci. Technol.*, 1991, vol. 7, pp. 307–10.
6. M. Nomura, H. Morimoto, and M. Toyama: *ISIJ Int.*, 2000, vol. 40, pp. 619–23.
7. D. Li, D. Anghelina, D. Burzic, J. Zamberger, R. Kienreich, H. Schifferi, W. Krieger, and E. Kozeschnik: *Steel Res. Int.*, 2009, vol. 80, pp. 298–303.
8. D. Li, D. Anghelina, D. Burzic, W. Krieger, and E. Kozeschnik: *Steel Res. Int.*, 2009, vol. 80, pp. 304–10.
9. C. Zhang, Y. Liu, L. Zhou, C. Jiang, and J. Xiao: *Int. J. Miner. Metall. Mater.*, 2012, vol. 19, pp. 116–21.
10. C. Zhang, L. Zhou, and Y. Liu: *Int. J. Miner. Metall. Mater.*, 2013, vol. 20, pp. 720–24.
11. S. Choi and Y. Lee: *ISIJ Int.*, 2014, vol. 54, pp. 1682–89.
12. S. Choi and S. Zwaag: *ISIJ Int.*, 2012, vol. 52, pp. 549–58.
13. X. Shi, L. Zhao, W. Wang, B. Zeng, L. Zhao, Y. Shan, M. Shen, and K. Yang: *TransMater. Heat Treat.*, 2013, vol. 34 (7), pp. 47–52.
14. Y. Liu, W. Zhang, Q. Tong, and L. Wang: *ISIJ Int.*, 2014, vol. 54, pp. 1920–26.
15. Y. Liu, W. Zhang, Q. Tong, and Q. Sun: *Int. J. Iron Steel Res.*, 2016, vol. 23, pp. 1316–22.
16. F. Zhao, C.L. Zhang, Q. Xiu, Y. Tan, S. Zhang, and Y.Z. Liu: *Mater. Sci. Forum*, 2015, vol. 817, pp. 132–36.
17. F. Zhao, C.L. Zhang, and Y.Z. Liu: *Arch. Metall. Mater.*, 2016, vol. 61, pp. 1715–22.
18. N. Birks: *Decarburization*, ISI Publication, Philadelphia, 1969, pp. 1–12.
19. N. Birks and W. Jackson: *J. Iron Steel Inst.*, 1970, vol. 208, pp. 81–85.
20. N. Birks, G. Meier, and F.S. Pettit: *Introduction to the High-Temperature Oxidation of Metals*, 1st ed., Edward Arnold, London, 1983, pp. 175–84.
21. N. Birks, G. Meier, and F.S. Pettit: *Introduction to the High-Temperature Oxidation of Metals*, 2nd ed., Cambridge University Press, Cambridge, 2006, pp. 151–62.
22. R.Y. Chen and W.Y.D. Yuen: in *Developments in High-Temperature Corrosion and Protection of Materials*, W. Gao and Z. Li, eds., Woodhead Publishing Limited, Cambridge, 2008, pp. 192–252.
23. R.Y. Chen and W.Y.D. Yuen: *ISIJ Int.*, 2005, vol. 45, pp. 52–59.
24. R.Y. Chen and W.Y.D. Yuen: *Metall. Mater. Trans. A*, 2009, vol. 40A, pp. 3091–3107.
25. W.S. Cao, S.-L. Chen, F. Zhang, K. Wu, Y. Yang, Y.A. Chang, R. Schmid-Fetzer, and W.A. Oates: *Calphad*, 2009, vol. 33, pp. 328–42.
26. PanFe. *Thermodynamic database for Fe-based alloys*, CompuTherm, LLC: Middleton WI 53562 (2019).
27. W. Jost: *Diffusion in Solids, Liquids and Gases*, Academic Press Inc, New York, 1960, pp. 69–71.
28. R.P. Smith: *Trans. Metall. Soc. AIME*, 1962, vol. 224, pp. 105–11.
29. A.E. Lord, Jr and D.N. Beshers: *Acta Melall.*, 1966, vol. 14, pp. 1659–72.
30. R.Y. Chen: *Oxid. Metals*, 2018, vol. 89, pp. 1–31.
31. R. Collin, S. Gunnarson, and D. Thulin: *J. Iron Steel Inst.*, 1972, vol. 210, pp. 785–89.
32. R.M. Asimov: *Trans. Metall. Soc. AIME*, 1964, vol. 230, pp. 611–13.
33. R.P. Smith: *Acta Metall.*, 1953, vol. 1, pp. 578–87.
34. C. Wells, W. Batz, and R.F. Mehl: Transactions AIME, 1950, vol. 188, Journal of MetalsTransactions, 1951, vol. 2, pp. 553–60.
35. G. Parrish and G.S. Harper: *Production Gas Carburising*, Pergamon Press, Oxford, 1985, pp. 114–16.
36. M.A. Krishtal, Diffusion processes in iron alloys, Israel Program for Scientific Translations, Jerusalem, pp. 90–133 (1970).
37. S.S. Babu and H.K.D.H. Bhadeshia: *J. Mater. Sci. Lett.*, 1995, vol. 14, pp. 314–16.
38. S.-J. Lee, D.K. Matlock, and C.J. Von Tyne: *ISIJ Int*, 2011, vol. 51, pp. 1903–11.
39. S.-J. Lee, D.K. Matlock, and C.J. Van Tyne: *Script. Mater.*, 2011, vol. 64, pp. 805–08.

40. S.K. Roy, H.J. Grabke, and W.W. Düsseldorf: *Arch. Eisenhütten-wess*, 1980, vol. 51, pp. 91–96.
41. H.K.D.H. Bhadeshia: *Metall. Mater. Trans. A*, 2010, vol. 41A, pp. 1605–15.
42. L.S. Darken: *Trans. AIME*, 1949, vol. 180, pp. 430–38.
43. M. E. Blanter, Diffusion processes in austenite and hardenability of alloyed steels, Thesis, Moskovski Institut Stali, Moscow, (1949).
44. J.K. Stanley: *Metal Trans.*, 1949, vol. 185, pp. 752–61.
45. C.G. Homan: *Acta Metall.*, 1964, vol. 12, pp. 1071–79.
46. A.A. Vasilyev and P.A. Golikov: *Mater. Phys. Mech.*, 2018, vol. 39, pp. 111–19.
47. R.B. Mclellan and P. Chraska: *Mater. Sci. Eng.*, 1971, vol. 7, pp. 305–17.
48. D.E. Jiang and E.A. Carter: *Phys. Rev. B*, 2003, vol. 67, p. 214103.
49. A. Pelton, P. Koukkari, R. Pajarre, and G. Eriksson: *J. Chem. Thermodyn.*, 2014, vol. 72, pp. 16–22.
50. M. Hillert: *Phase Equilibria, Phase Diagrams and Phase Transformation – Their Thermodynamic Basis*, 2nd ed., Cambridge University Press, Cambridge UK, 2008, pp. 311–15.
51. J. Takada and M. Adachi: *J. Mater. Sci.*, 1986, vol. 21, pp. 2133–37.
52. H. Li, J. Zhang, and D.J. Young: *Mater. High Temp.*, 2011, vol. 28, pp. 297–301.
53. H. Li, J. Zhang, and D.J. Young: *Corros. Sci.*, 2012, vol. 54, pp. 127–38.
54. K. Kusabiraki, R. Watanabe, T. Ikehata, M. Takeda, T. Onishi, X. Guo, and H. Anada: *Tetsu-to-Hagane*, 2007, vol. 93, pp. 379–85 (in Japanese).
55. K. Kusabiraki, R. Watanabe, T. Ikehata, M. Takeda, T. Onishi, X. Guo, and H. Anada: *ISIJ Int.*, 2007, vol. 47, pp. 1329–34.
56. F.D. Richardson and J.H.E. Jeffes: *J. Iron Steel Inst.*, 1948, vol. 160, pp. 261–70.
57. O. Kubaschewski and C.B. Alcock: *Metallurgical Thermochemistry*, 5th ed., Pergamon Press, Oxford, 1979, p. 379.
58. J.A. Lobo and G.H. Gaiger: *Metall. Trans. A*, 1976, vol. 7A, pp. 1347–57.
59. Y.R. Chen, X. Xu, and Y. Liu: *Oxid. Metals*, 2020, vol. 93, pp. 105–29.